Supporting Information

Trace Cobalt Inserted Platinum Lattice Gap to Enable Bifunctional Oxygen Electrocatalysis

Jie Yang[a], Shilong Song[a], Zhanwei Chen[a], Bo Zhang[a], Yuyu Guo [a]*, Ying Guo[a]* and Hepeng Zhang[a]*

[a] Xi'an Key Laboratory of Functional Organic Porous Materials, School of Chemistry and Chemical Engineering, Northwestern Polytechnical University.

Xi'an 710129, PR China

* Corresponding Author

Table of Contents

1. Experimental Section
2. Supporting Figures and Tables
3. Reference

1. Experimental Section

1.1. Materials and reagents

Dimethyl imidazole (MeIM), dicyandiamide ($C_2H_4N_4$), D-(+)-Glucose ($C_6H_{12}O_6$), and chloroplatinic acid hexahydrate ($H_2PtCl_6·H_2O$), zinc acetate ($Zn(CH_3COO)_2$)were purchased from Aladdin Reagent Co., Ltd (Shanghai, China). Zinc nitrate hexahydrate ($Zn(NO_3)_2·6H_2O$), cobalt nitrate hexahydrate ($Co(NO_3)_2·6H_2O$), ferric nitrate nonahydrate ($Fe(NO_3)_3·9H_2O$), Potassium hydroxide (KOH, 85.0%), isopropanol, methanol, and ethanol were obtained from Guangdong Guanghua Technology Co., Ltd. Commercial Pt/C catalyst (20 wt%, hispec 3000) was obtained from Johnson Matthey. Nafion solution (5 wt%) was purchased from Sigma-Aldrich LLC. The gas used in experiments: high-purity oxygen (O_2, >99.999%), high-purity nitrogen (N_2, >99.999%) and high-purity carbon monoxide (CO, >99.999%). All the above reagents are of analytical grade and are used directly without further purification before the experiment. Deionized water used in the experiments was obtained locally.

1.2. Catalysts preparation

1.2.1. Preparation of Zn-ZIF precursors

During the typical synthesis procedure, 7.5 mmol $Zn(NO_3)_2·6H_2O$ was dispersed in 75 mL methanol. This solution was then quickly poured into a solution of 30.0 mmol MeIM in methanol. After ultrasonic mixing for 10 minutes, the resulting slurry was stirred at room temperature for 12 hours. The solids obtained were centrifugally washed with ethanol several times and then dried under vacuum at 60 °C overnight. The products obtained were labeled as Zn-ZIF.

1.2.2. Preparation of NC precursors

The as-synthesized Zn-ZIF was put into in a tubular furnace and heated from room temperature to 1000 °C at a heating rate of 5 °C min^{-1}, and kept for 2 h under N_2 flow.

1.2.3. Preparation of Fe-N-C

The 100 mg as-synthesized NC precursors, 10 mg $Fe(NO_3)_3·9H_2O$ and 10 mg dicyandiamide ($C_2H_4N_4$) were poured into a solution of 10 mL isopropanol. After ultrasonic mixing for 2 h, the obtained solution was centrifuged and then dried under

vacuum at 60 °C overnight. The dried product was put into in a tubular furnace and heated from room temperature to 900 °C at a heating rate of 5 °C min^{-1}, and kept for 2 h under N_2 flow. The product obtained were labeled as Fe-N-C.

1.2.4. Preparation of Pt@Fe-N-C

The 50 mg as-synthesized Fe-N-C, 21 mg $H_2PtCl_6 \cdot H_2O$, and 15 mg D-(+)-Glucose ($C_6H_{12}O_6$) were poured into 25 mL DI water. After ultrasonic mixing for 5 min, the obtained solution was reacted at 200 °C for 24 h. The solution was centrifuged and then dried under vacuum at 60 °C overnight. The products obtained were labeled as Pt@Fe-N-C.

1.2.5. Preparation of Co@Fe-N-C

The 50 mg as-synthesized Fe-N-C, 16.1 mg $Co(NO_3)_2 \cdot 6H_2O$, and 15 mg D-(+)-Glucose ($C_6H_{12}O_6$) were poured into 25 mL DI water. The rest of the experimental steps are the same as for the preparation of Pt@Fe-N-C. The products obtained were labeled as Co@Fe-N-C.

1.2.6. Preparation of Co-Pt@Fe-N-C

The 50 mg as-synthesized Fe-N-C, 21 mg $H_2PtCl_6 \cdot H_2O$, 16mg $Co(NO_3)_2 \cdot 6H_2O$ and D-(+)-Glucose ($C_6H_{12}O_6$) were poured into 25 mL deionized water. After ultrasonic mixing for 5 minutes, the obtained solution was reacted at 200 °C for 24 h. The solution was centrifuged and then dried under vacuum at 60 °C overnight. The products obtained were labeled as Co-Pt@Fe-N-C.

1.3. Characterizations

Powder X-ray diffraction (XRD) patterns of the catalysts were recorded on a Bruker D8 DISCOVER A25 X-ray diffractometer (Germany) with Pt K α radiation (3 kV). The samples' morphology and structure were studied using transmission electron microscopy (TEM, FEI Talos F200X TEM operated at 200 kV). The high-angle annual dark-filed scanning transmission electron microscopy (HAADF-STEM) and energy dispersive X-ray spectroscopy (EDS) were performed on an FEI Themis Z microscope equipped with spherical aberration corrector and operated at 300 kV, with a guaranteed resolution of 0.06 nm. The actual content of Pt, Co and Fe were obtained on an Inductively Coupled Plasma Atomic Emission Spectrometry (ICP-AES,

NexION™ 350D PerkinElmer USA). Attenuated Total Reflectance Fourier-Transform Infrared (ATR-FTIR) spectra and Diffuse Reflectance Infrared Fourier Transform (DRIFT) spectra were tested through Infrared Spectroscopy (IR, Nicolet™ iS20 FTIR Spectrometer). X-ray photoelectron spectroscopy (XPS) measurements were performed with an Axis Ultra DLD X-ray photoelectron spectroscopy manufactured by Kratos Company in the United Kingdom. The instrument used an Al K ray light source to measure the total ambient gas pressure ($<10^{-8}$ Pa). The X-ray absorption fine structure spectra at the Pt L-edge were collected at the BL14W beamline of the Shanghai Synchrotron Radiation Facility (SSRF). The facility's storage rings were operating at 3.5 GeV with a consistent current of 200 mA. Data collection was performed in transmission mode using a Si (111) double-crystal monochromator, with all spectra being gathered under ambient conditions.

Extended X-ray absorption fine structure (EXAFS) Fitting:

Fitting of the EXAFS region was performed using the Artemis program of the IFEFFIT package. Fitting was performed in R space, with a L-weight of 2 for all the Pt samples. Refinement was performed by optimizing an amplitude factor S_0^2 and energy shift ΔE_0 which are common to all paths, in addition to parameters for bond length (ΔR) and Debye-Waller factor (σ^2). The fitting model for Co-Pt@Fe-N-C were based on the DFT optimized structure.

1.4. Electrochemical measurements

Electrochemical measurements were carried out using an electrochemical workstation (Metrohm Multi Auto-lab/M204) with a standard three-electrode cell and a rotating disk electrode (RDE) system. The RDE system, with a glassy carbon disk of 5 mm in diameter, was used as the working electrode. To prepare the ink, 5 mg of catalyst was ultrasonically dispersed in a 1.0 mL mixture of ethanol (90 μL), water (900 μL) and Nafion (5 wt.%, 10 μL) solution to form an ink. Then 10 μL of the ink was drop-cast on the working electrode and dried at room temperature. An Ag/AgCl (saturated KCl) electrode was used as the reference electrode, and a graphite rod as the counter electrode. A 0.1 M KOH aqueous solution was used as electrolyte. The electrolyte was purged with required gas for at least 30 min before the test, with the gas flow

maintained during the test. The ORR performance was measured in an O_2-saturated 0.1 M KOH solution with a 1,600 r.p.m. rotation rate at 10 mV s^{-1}. The kinetic current density can be calculated from the Koutecky-Levich (K-L) equation[2]:

$$\frac{1}{J} = \frac{1}{J_L} + \frac{1}{J_K} = \frac{1}{B\omega^{1/2}} + \frac{1}{J_K}$$
$$B = 0.62nFC_0D_0^{2/3}v^{-1/6}$$

where J is the measured current density, J_K and J_L are the kinetic and diffusion-limiting current densities, ω is the angular velocity, n is transferred electron number, F is the Faraday constant (96, 485 C mol^{-1}), C_0 is the bulk concentration of O_2 (1.26×10^{-6} mol cm^{-3}), D_0 is the diffusion coefficient of O_2 (1.90×10^{-5} cm^2 s^{-1}), and v is the kinematic viscosity of the electrolyte (0.01 cm^2 s^{-1}).

The number of transfer electrons (n) and hydrogen peroxide yield were determined on rotating ring disk electrode (RRDE) by the following equation:

$$H_2O_2(\%) = 200 \times \frac{\dfrac{I_r}{N}}{I_d + \dfrac{I_r}{N}}$$

$$n = 4 \times \frac{I_d}{I_d + \dfrac{I_r}{N}}$$

Where I_d and I_r represent the disk current and ring current, respectively. N is the current collection efficiency of Pt ring towards intermediate reaction and defined as 0.25.

For OER, 5 mg of catalyst was ultrasonically dispersed in a 1.0 mL mixture of isopropanol (750 µL), water (200 µL) and Nafion (5 wt.%, 50 µL) solution to form the ink. Then 100 µL of the ink was sprayed onto a 1×1 cm^2 carbon paper to achieve a loading of 0.25 mg cm^{-2} as the working electrode. A 0.1 M KOH aqueous solution was used as the electrolyte. A linear sweep voltammetry technique was applied during the activity evaluation, and the curves were recorded at a scan rate of 5 mV s^{-1}. For electrochemical tests, all the potentials were referred to a RHE based on the equation:

E (versus RHE) = E (versus Ag/AgCl) + 0.197 V + 0.059 V × pH.

Assembly of aqueous Zn-air batteries: 5 mg of electrocatalyst samples were dispersed in 750 µL purified water, 200 µL ethanol and 50 µL Nafion solution (5

wt%) to form a homogeneous catalyst ink. Then, 200 μL electrocatalyst ink was dropped onto a hydrophobic carbon paper (1cm^2) as the air-cathode. Meanwhile, Zn-foil and 6 M KOH/0.2 M Zn(CH$_3$COO)$_2$ served as the anode and electrolyte, respectively. The discharge polarization curves and corresponding power density plots of Co-Pt@Fe-N-C, Pt@Fe-N-C and Pt/C based ZAB were tested on a CS350H electrochemical workstation (Wuhan Corrtest Instruments Corp., Ltd.). The performance of the batteries was measured by LAND-CT2001A system.

1.5. In situ ATR-FTIR measurements

The catalyst ink was applied uniformly onto a 2 × 2 cm^2 carbon paper to prepare the working electrode (1 mg catalyst cm^{-2}). For the oxygen reduction reaction (ORR), before the *in-situ* ATR-FTIR test, the electrode underwent potential cycling in 0.1 M KOH by cyclic voltammetry between - 0.76 V to 0.24 V (vs. Ag/AgCl) with 10 mVs^{-1} until stable voltammograms were obtained. Additionally, graphite rod was used as a counter electrode, and Ag/AgCl was used as a reference electrode. Subsequently, the electrode was immersed in a 30 mL electrolyte containing 0.1 M KOH in the spectra electrochemical setup. O$_2$ was bubbling to the electrolyte in advance and continuously bubbled throughout the experiment. The IR test was conducted by ThermoFisher scientific iS20 with a liquid N$_2$-cooled MCT (mercury cadmium telluride) detector using a VeeMax III ATR accessory (Pike Technologies). The obtained carbon paper was fixed above the Si crystal and connected with a glassy carbon electrode. A CHI 760E electrochemical workstation (CH Instruments, USA) was connected for chronoamperometric tests from 0.2 to 1.1 V *vs.* RHE stepwise. The spectra under open circuit potential (OCP) were recorded for comparison. For the oxygen evolution reaction (OER), just change the chronoamperometric tests from 1.2 to 1.8 V *vs.* RHE stepwise.

1.6. Computational methods

We have employed the VASP[1, 2] to perform all the density functional theory (DFT) calculations within the generalized gradient approximation (GGA) using the Perdew-Burke-Ernzerhof (PBE)[3] formulation. We have chosen the projected augmented wave

(PAW) potentials[4] to describe the ionic cores. Take valence electrons into account using a plane wave basis set with a kinetic energy cutoff of 450 eV. Partial occupancies of the Kohn-Sham orbitals were allowed using the Gaussian smearing method and a width of 0.05 eV. The electronic energy was considered self-consistent when the energy change was smaller than 10^{-5} eV. A geometry optimization was considered convergent when the energy change was smaller than 0.05 eV Å^{-1}. The brillouin zone is sampled with $3 \times 3 \times 1$ Monkhorst mesh[5].

Gibbs free energy can be obtained by adding corrections including entopic (TS) and zero-point energy (ZPE) to calculated DFT energy, so that $\Delta G = \Delta E_{DFT} + \Delta ZPE - T\Delta S - eU$.

where the E_{DFT} is the calculated DFT reaction energy, ΔZPE is the change in ZPE calculated from the vibrational frequencies and ΔS is the change in the entropy referring to thermodynamics databases. The electrode potential are adopted with respect to the reversible hydrogen electrode, which makes the standard electrochemical potential of electron involved in reaction (G_e) equal to -eU, and the standard electrochemical potential of the proton (G_{H+}) equal to that of the hydrogen atom in gaseous H_2 ($1/2G_{H2}$). Considering that the triplet state of the O_2 molecule is poorly described in the current DFT scheme, the free energy of the O_2 molecule was derived according to $G_{O2} = 2G_{H2O} - 2G_{H2} + 4.92$.

2. Figures and Tables

Supplementary Figures
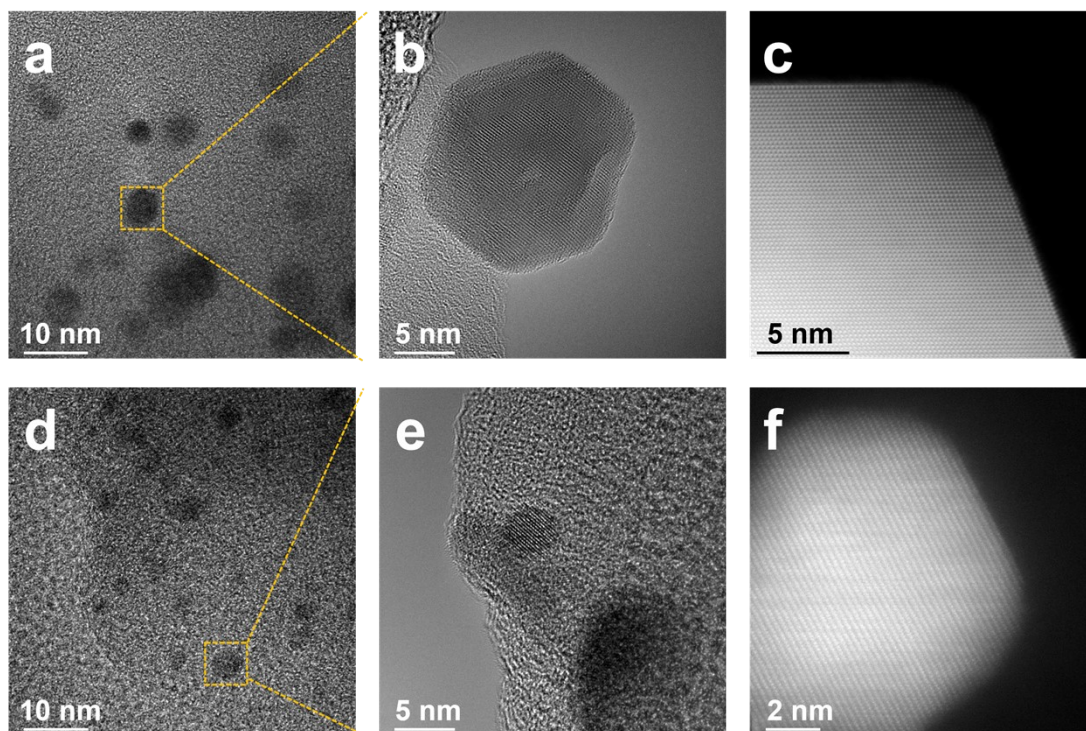
Figure S1. (a), (b) TEM images of the Co-Pt@Fe-N-C; **(c)** HAADF-STEM images of the Co-Pt@Fe-N-C; **(d), (e)** TEM images of the Pt@Fe-N-C and **(f)** HAADF-STEM images of the Pt@Fe-N-C.
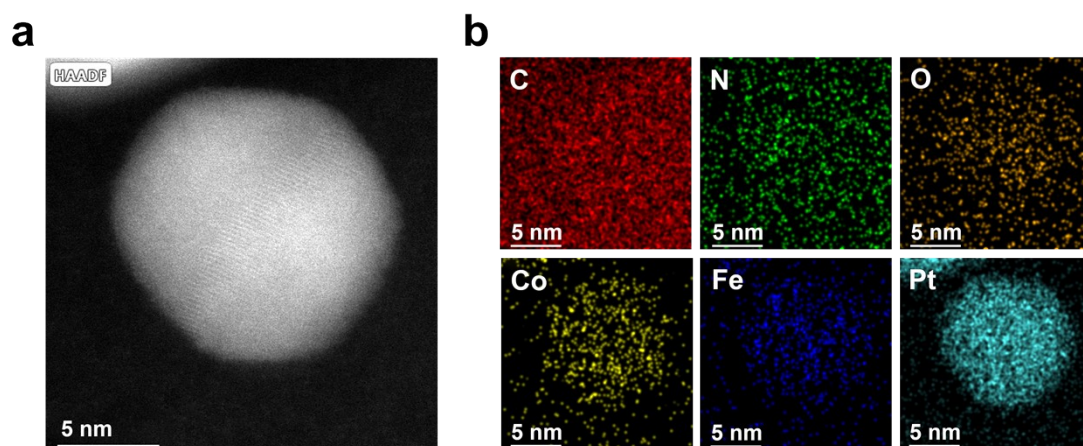
Figure S2. (a) HAADF-STEM images of the Co-Pt@Fe-N-C; **(b)** Elemental mapping images of the Co-Pt@Fe-N-C.
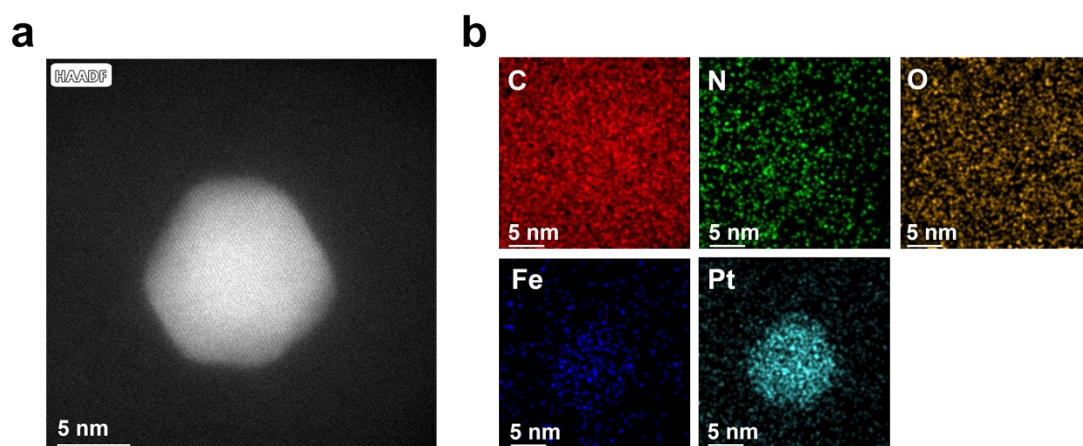
Figure S3. (a) HAADF-STEM images of the Pt@Fe-N-C; **(b)** Elemental mapping images of the Pt@Fe-N-C.
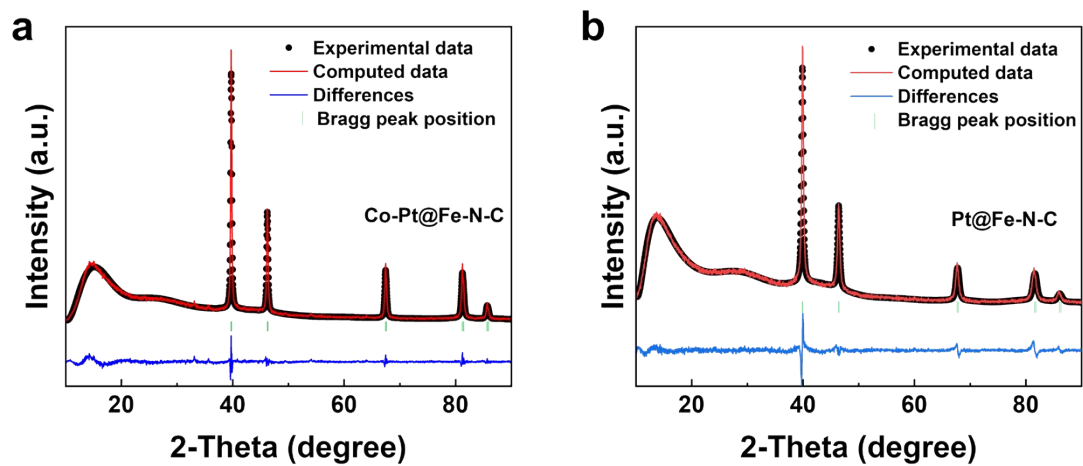
Figure S4. (a) Rietveld refinement profile for Co-Pt@Fe-N-C; **(b)** Rietveld refinement profile for Pt@Fe-N-C.

a

d=0.216 nm
(1 1 1)

2 nm

b

0.05

0

-0.05
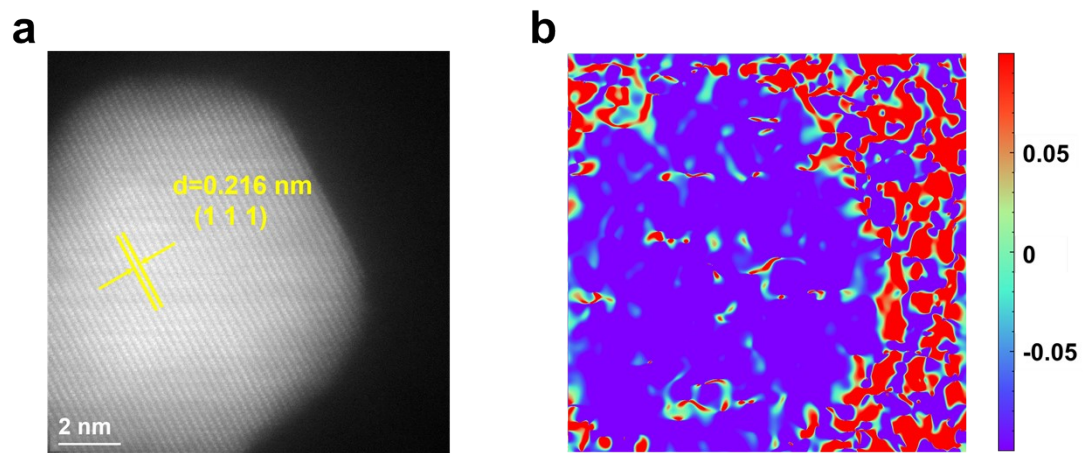
Figure S5. (a) HAADF-STEM images of the Pt@Fe-N-C; **(b)** ε_{xx} strain component determined via GPA of Pt@Fe-N-C.
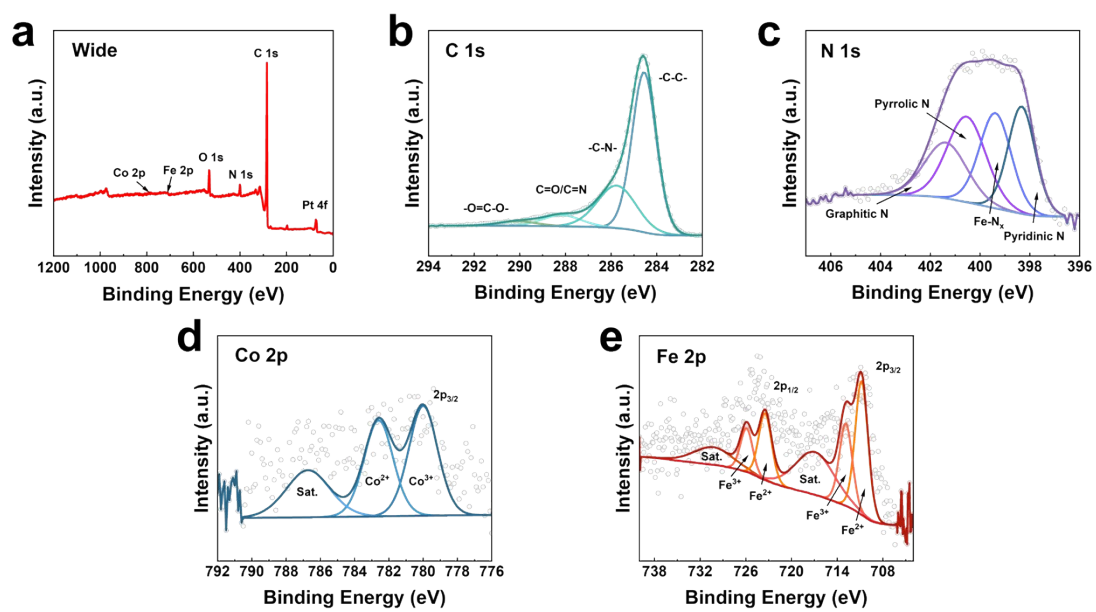
Figure S6. (a) XPS wide, **(b)** C 1s, **(c)** N 1s, **(d)** Co 2p and **(e)** Fe 2p spectra of Co-Pt@Fe-N-C.
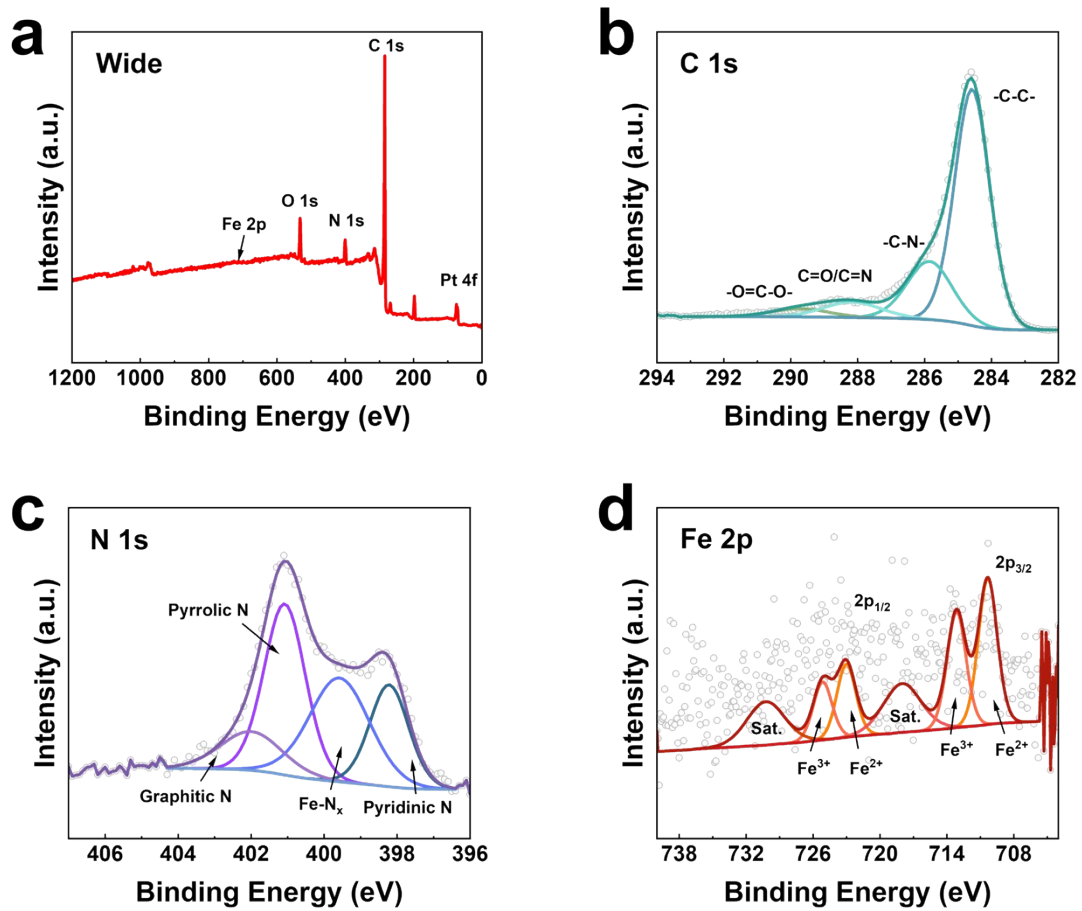
Figure S7. (a) XPS wide, **(b)** C 1s, **(c)** N 1s, and **(d)** Fe 2p spectra of Pt@Fe-N-C.
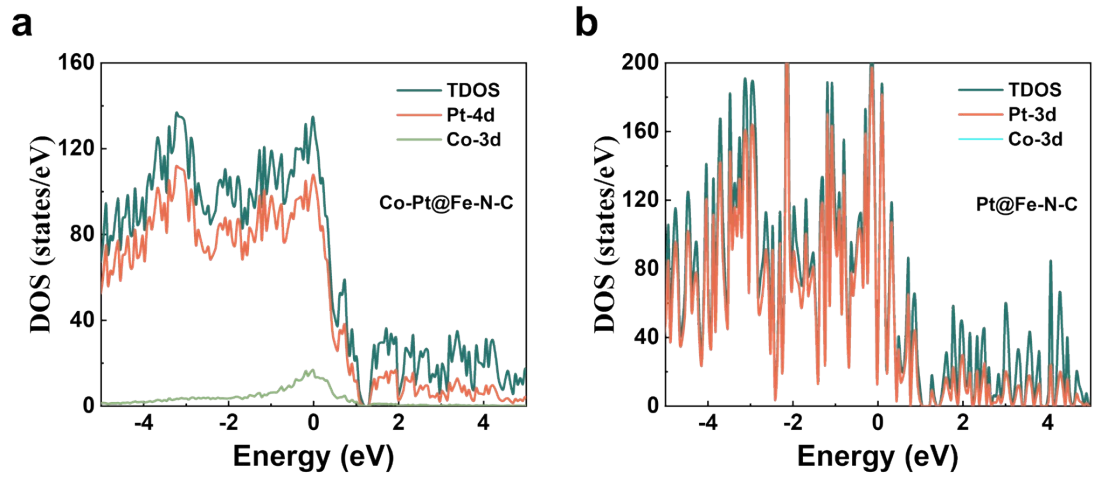
Figure S8. The density of states (DOS) and partial density of states of Pt and Co in **(a)** Co-Pt@Fe-N-C; **(b)** Pt@Fe-N-C.
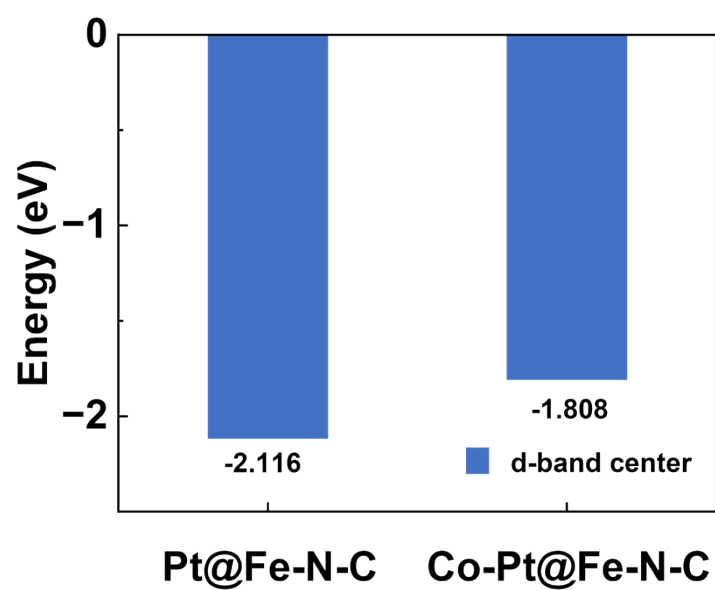
Figure S9. The comparison of d-band centers for Co-Pt@Fe-N-C and Pt@Fe-N-C.
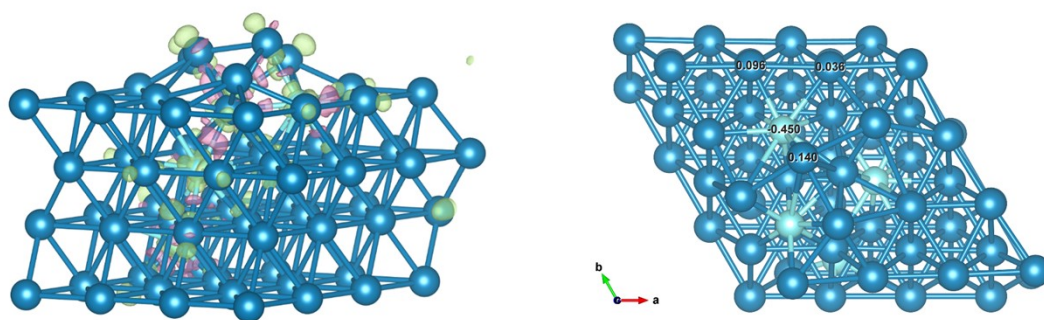
Figure S10. Difference charge density of Co-Pt@Fe-N-C.
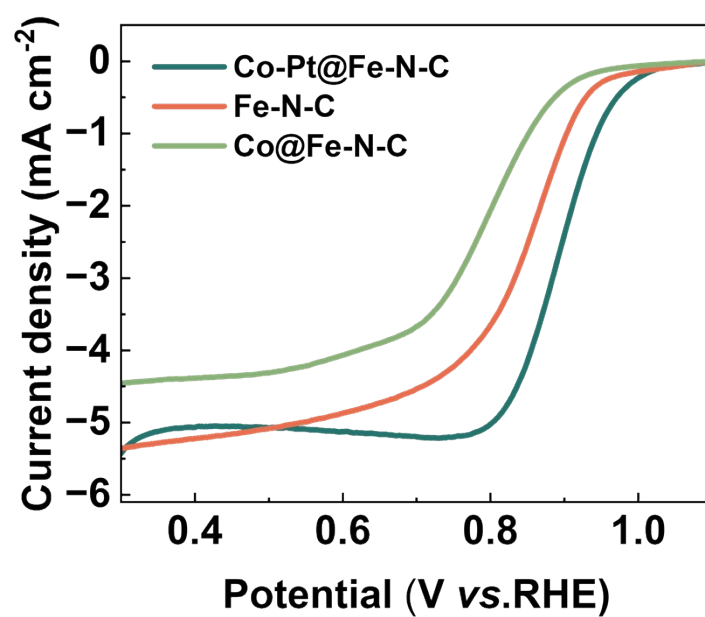
Figure S11. ORR LSV polarization curves of Co-Pt@Fe-N-C, Co@Fe-N-C and Fe-N-C.
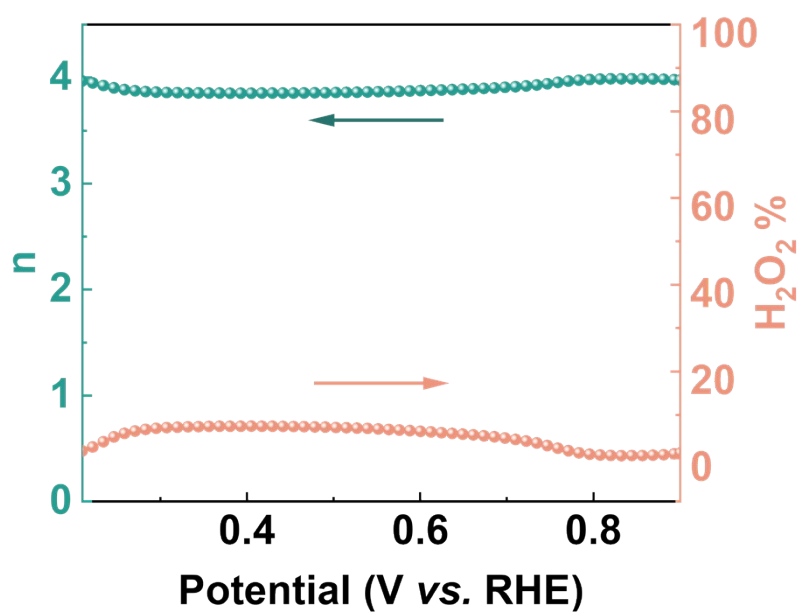
Figure S12. Hydrogen peroxide yield and corresponding electron transfer number of Co-Pt@Fe-N-C at different potentials.
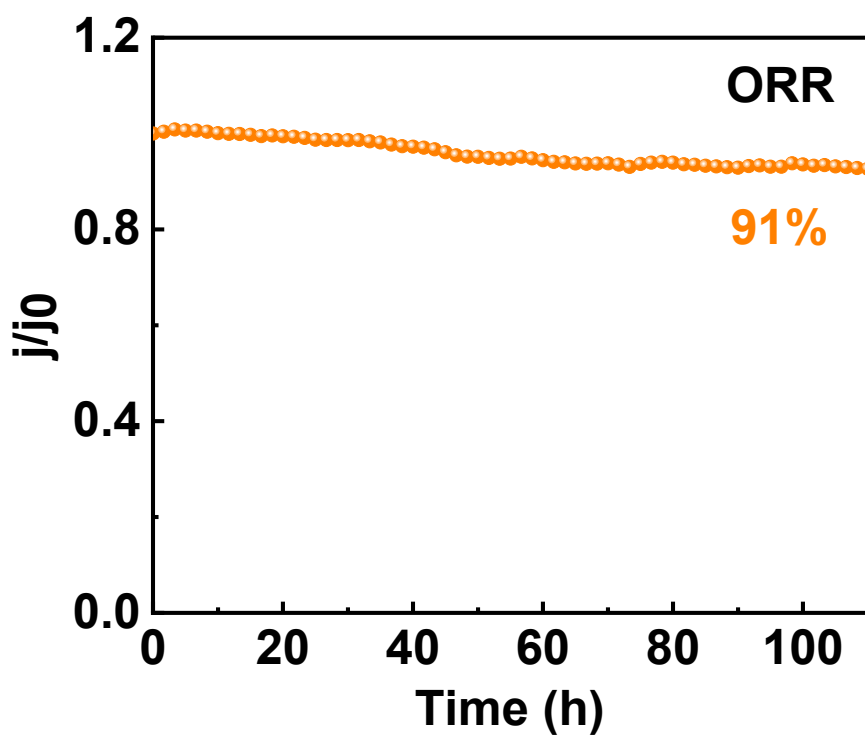
Figure S13. Chronoamperometric curves of Co-Pt@Fe-N-C for ORR.
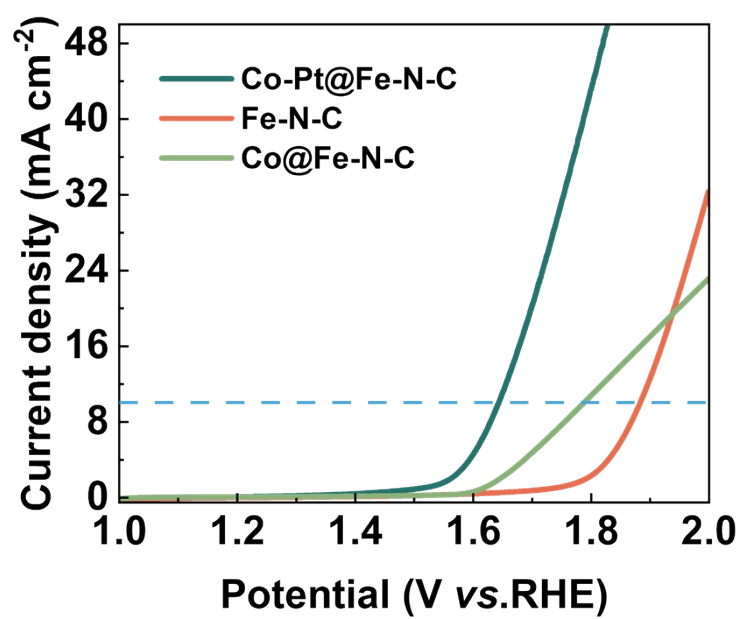
Figure S14. OER LSV polarization curves of Co-Pt@Fe-N-C, Co@Fe-N-C and Fe-N-C.
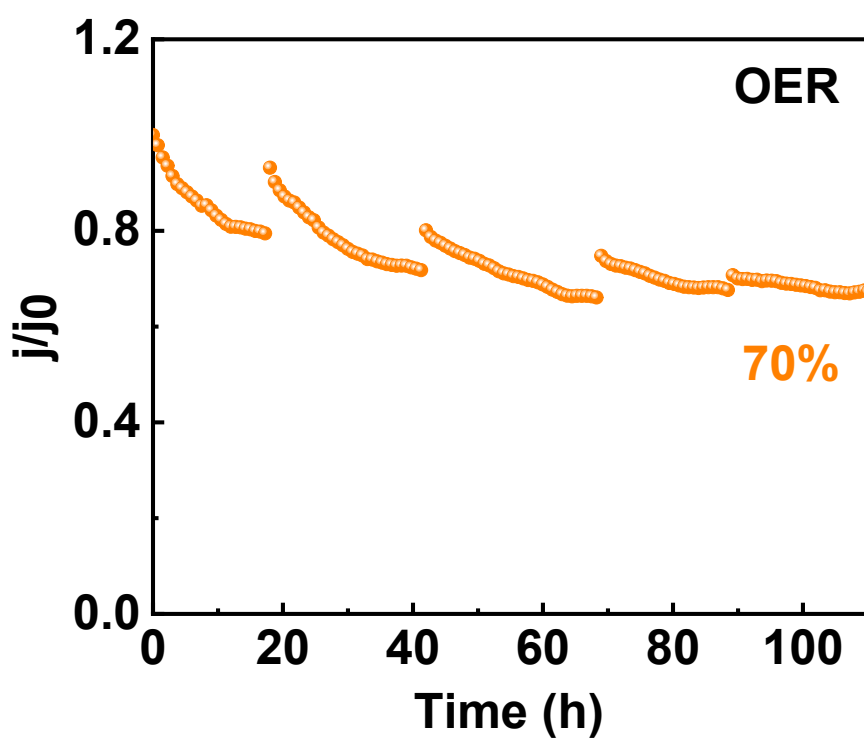
Figure S15. Chronoamperometric curves of Co-Pt@Fe-N-C for OER.
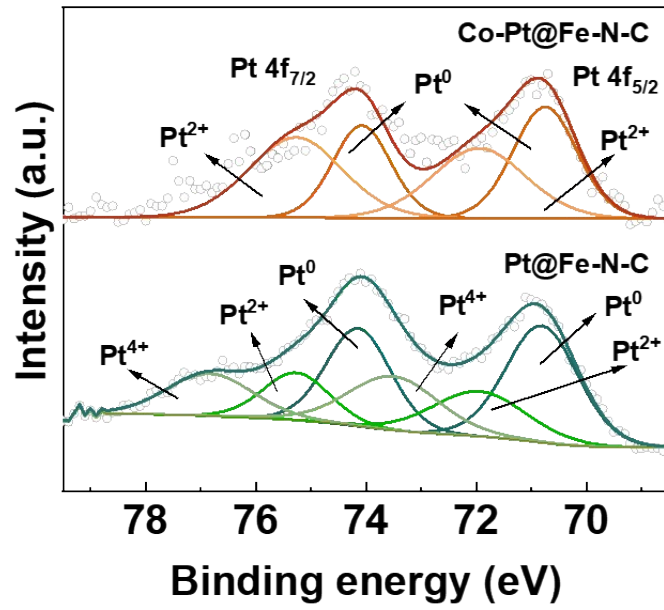
Figure S16. XPS results of Pt 4f spectra of Co-Pt@Fe-N-C and Pt@Fe-N-C after OER stability testing.
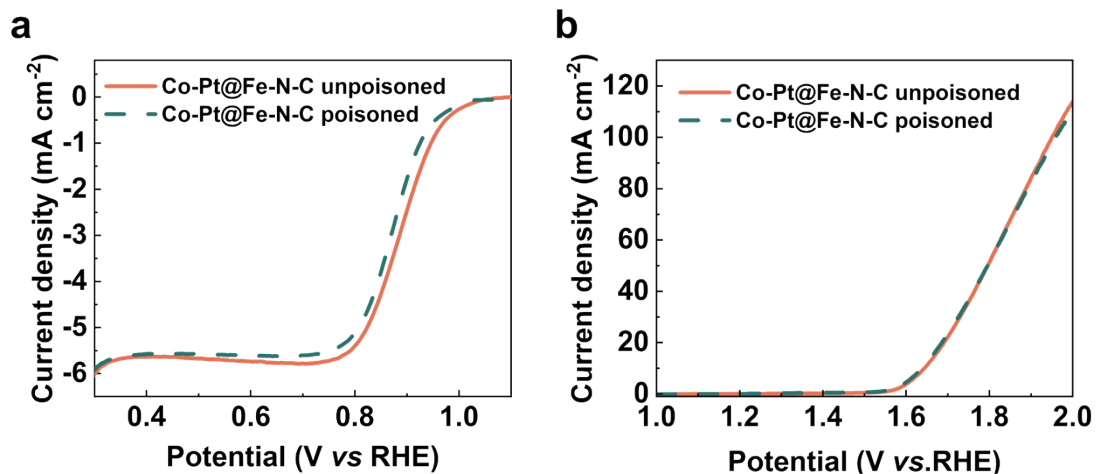
Figure S17. a) ORR LSV polarization curves of Co-Pt@Fe-N-C before and after addition of 0.01 M KSCN in electrolyte; **b)** OER LSV polarization curves of Co-Pt@Fe-N-C before and addition of 0.01 M KSCN in electrolyte.

Figure S18. Digital photo of OCP measured by multimeter of ZABs using **(a)** Co-Pt@Fe-N-C, **(b)** Pt@Fe-N-C and **(c)** Pt/C as catalysts.
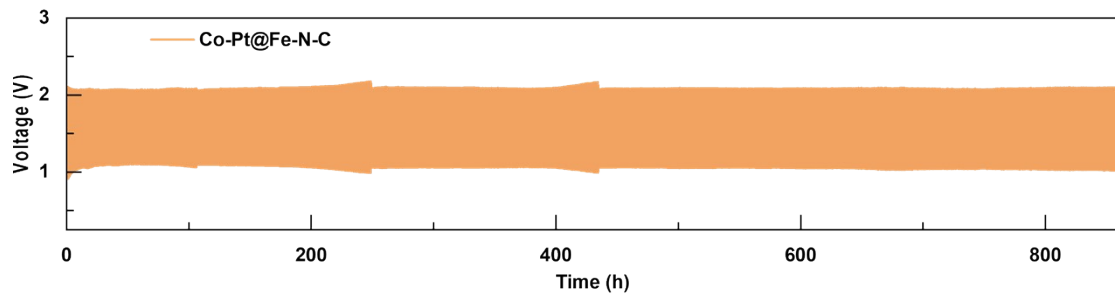
Figure S19. Galvanostatic discharging and charging curves of Co-Pt@Fe-N-C at 10 mA cm^{-2}.
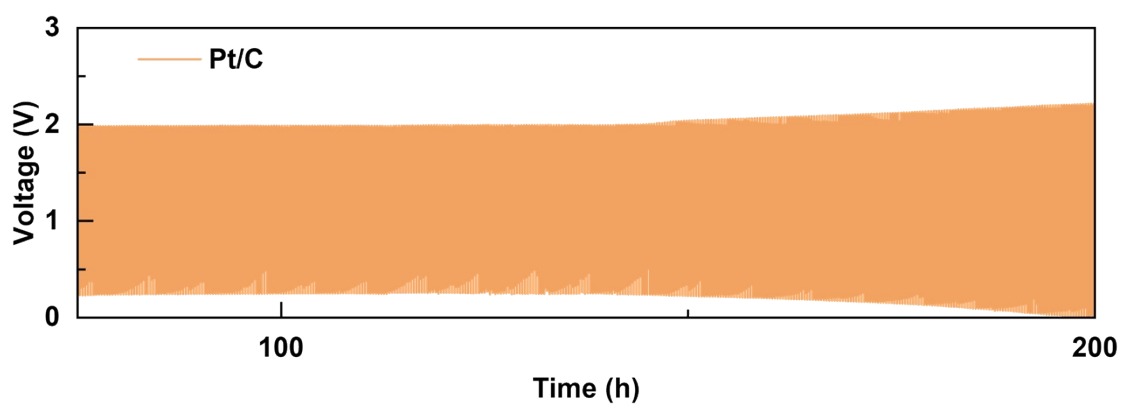
Figure S20. Galvanostatic discharging and charging curves of Pt/C at 10 mA cm^{-2}.
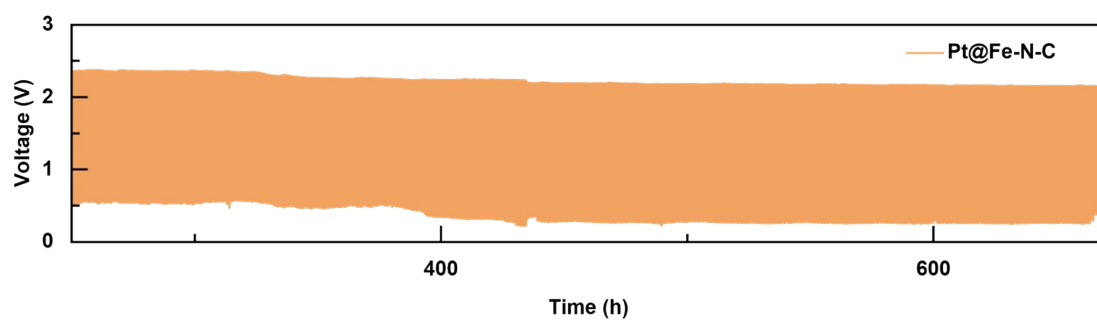
Figure S21. Galvanostatic discharging and charging curves of Pt@Fe-N-C at 10 mA cm^{-2}.
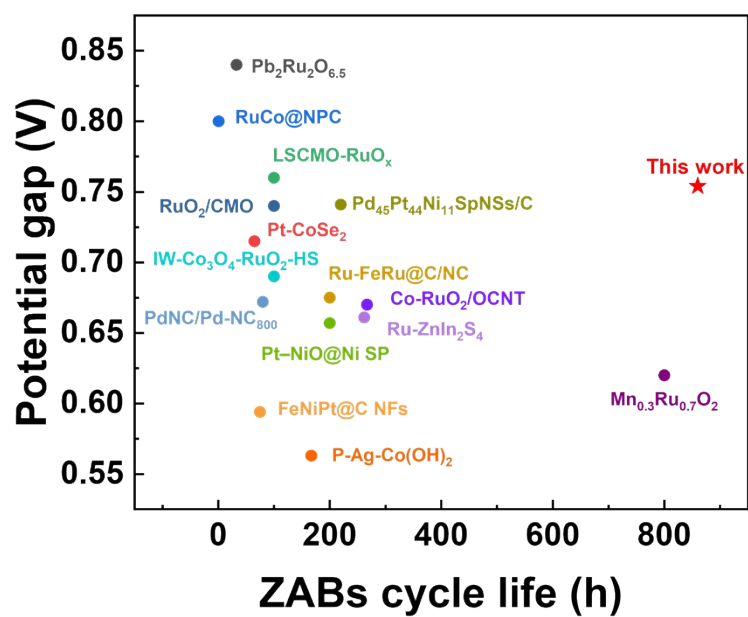
Figure S22. The comparison of ORR and OER performance (potential gap) for reported catalysts with this work.
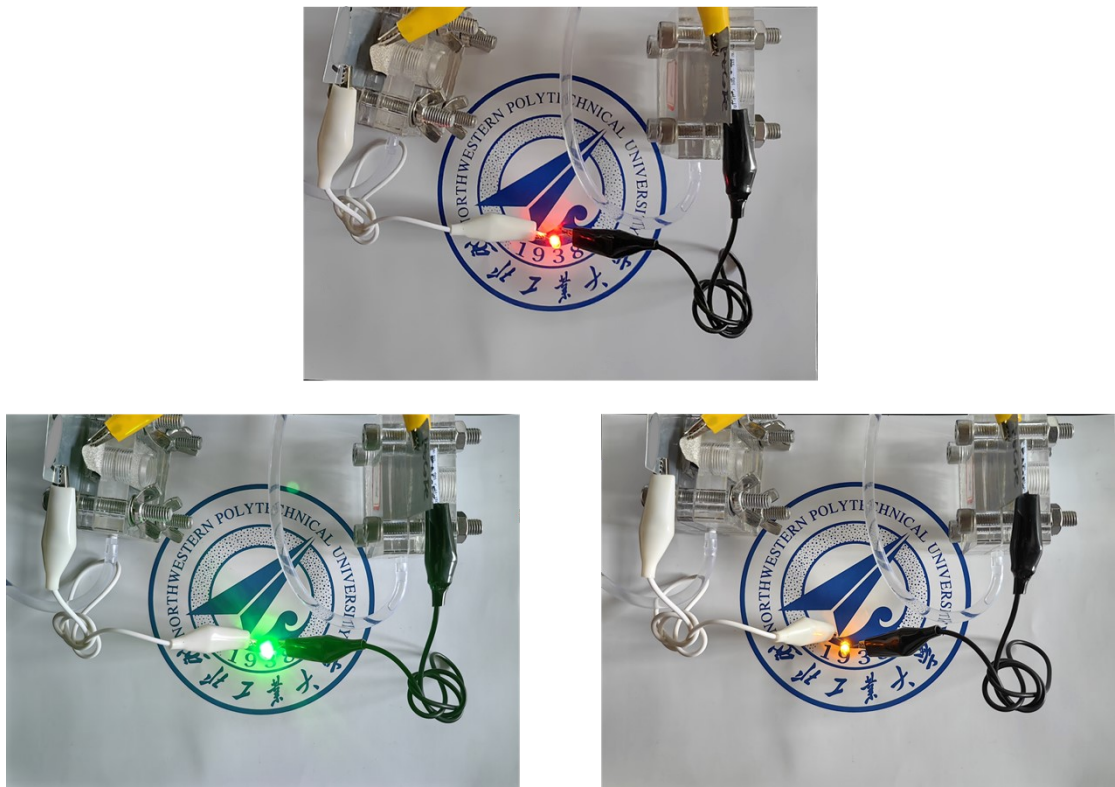
Figure S23. Using two self-assembled ZABs in series to power a bulb.
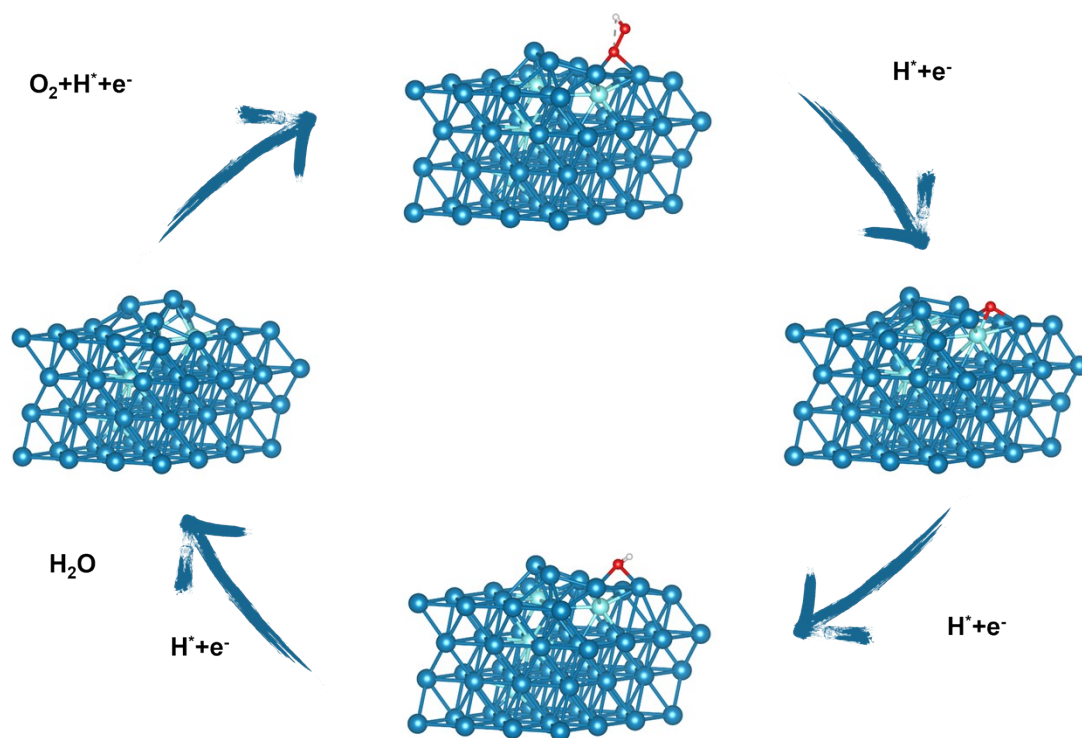
Figure S24. The reaction pathway of ORR on the model structures of Co-Pt@Fe-N-C.
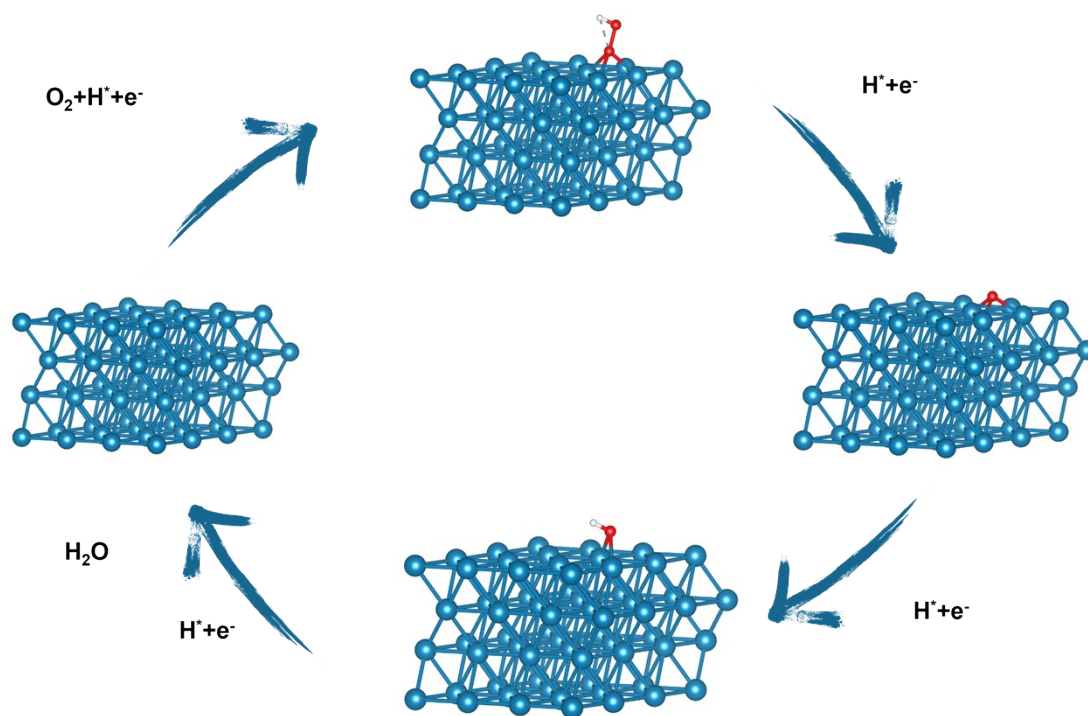
Figure S25. The reaction pathway of ORR on the model structures of Pt@Fe-N-C.

Supplementary Tables

Table S1. The metal content of Pt, Co, and Fe elements in Co-Pt@Fe-N-C, Pt@Fe-N-C, and Pt/C measured by ICP-AES.

Sample	Pt (wt%)	Co (wt%)	Fe (wt%)
Co-Pt@Fe-N-C	10.28	0.22	2.49
Pt@Fe-N-C	12.08	/	4.71
Pt/C	20	/	/

Table S2. The Rietveld refinement results of Co-Pt@Fe-N-C and Pt@Fe-N-C.

Sample	Pt	Pt@Fe-N-C	Co-Pt@Fe-N-C
a (Å)	3.9231	3.9096	3.9235
b (Å)	3.9231	3.9096	3.9235
c (Å)	3.9231	3.9096	3.9235
α (°)	90	90	90
β (°)	90	90	90
γ (°)	90	90	90
R_p	/	4.18	4.83
R_{wp}	/	5.96	6.19
Expansion	/	-1.02	0.03

Table S3. Structure parameters of related samples extracted of the EXAFS fitting.

Sample	R_{Pt-Pt} (Å)	N_{Pt-Pt}	σ^2_{Pt-Pt}(Å^2)	E_0(eV)	R factor
Co-Pt@Fe-N-C	2.7580	12	0.0053	6.7000	0.0139
Pt foil	2.7530	12	0.0058	6.0494	0.0142

Sample	R_{Pt-O}(Å)	N_{Pt-O}	σ^2_{Pt-O}(Å^2)	E_0(eV)	R factor
PtO$_2$	2.0046	6	0.0025	9.9143	0.0137

Table S4. Dissolved amount of Pt (mg/L) in Co-Pt@Fe-N-C catalysts during 100 hours of ORR and OER stability experiments.

ORR	0-20 h	20-40 h	40-60 h	60-80 h	80-100 h
Pt (mg/L)	0.012	0.003	0.003	0.002	0.001

OER	0-20 h	20-40 h	40-60 h	60-80 h	80-100 h
Pt (mg/L)	0.026	0.017	0.012	0.006	0.004

Table S5. Bifunctional activities of Co-Pt@Fe-N-C, Pt@Fe-N-C, and Pt/C.

Catalysts	ORR@$E_{1/2}$ (V)	OER@10 mA cm^{-2} (V)	ΔE (V)
Co-Pt@Fe-N-C	0.89	1.64	0.75
Pt@Fe-N-C	0.86	1.95	1.09
Co@Fe-N-C	0.79	1.79	1.00
Fe-N-C	0.83	1.88	1.05
Pt/C	0.85	1.85	1.00

Table S6. The comparison of ORR and OER performance as well as Zn-Air battery life for reported catalysts with this work.

Catalysts	ORR@$E_{1/2}$ (V)	OER@10 mA cm^{-2} (V)	ΔE (V)	Zn-Air battery life	Ref.
This work	0.89	1.644	0.754	860h	
$Pb_2Ru_2O_{6.5}$	0.81	1.65	0.84	33h	[6]
$Pt-CoSe_2$	0.83	1.545	0.715	65h	[7]
$RuCo@NPC$	0.78	1.58	0.8	16.7h	[8]
$La_{0.8}Sr_{0.2}Co_{0.5}Mn_{0.5}O_3-RuO_x$	0.76	1.48	0.76	100h	[9]
$Ru-ZnIn_2S_4$	0.845	1.506	0.661	262h	[10]
$Ru-FeRu@C/NC$	0.90	1.575	0.675	200h	[11]
$IW-Co_3O_4-RuO_2-HS$	0.79	1.48	0.69	100h	[12]
$Co-RuO_2/OCNT$	0.82	1.49	0.67	267h	[13]
$Pd_{45}Pt_{44}Ni_{11}SpNSs/C$	0.945	1.686	0.741	220h	[14]
$P-Ag-Co(OH)_2$	0.902	1.465	0.563	167h	[15]
$Pd_{NC}/Pd-NC_{800}$	0.85	1.522	0.672	80h	[16]
$Pt–NiO@Ni\ SP$	0.896	1.553	0.657	200h	[17]
$Mn_{0.3}Ru_{0.7}O_2$	0.85	1.47	0.62	800h	[18]
RuO_2/CMO	0.80	1.54	0.74	100h	[19]
$FeNiPt@C\ NFs$	0.93	1.524	0.594	75h	[20]

Table S7. Location of the infrared diffraction peaks (cm⁻¹) for ORR and OER reaction intermediates of Co-Pt@Fe-N-C and Pt@Fe-N-C.

	Catalysts	$^*O_2$	$^*OOH$	$^*O$	$^*OH$	H_2O
ORR	Co-Pt@Fe-N-C	1542	1168	871	1643	/
	Pt@Fe-N-C	1540	1164	840	1639	/
OER	Co-Pt@Fe-N-C	1531	1170	896	1654	/
	Pt@Fe-N-C	1529	1168	879	1644	/

Table S8. Synergistic OER and ORR electrocatalytic pathways of Co-Pt@Fe-N-C, Pt@Fe-N-C at 0 V.

Catalysts	ΔG_1	ΔG_2	ΔG_3	ΔG_4
Co-Pt@Fe-N-C	0.675	2.863	0.393	0.988
Pt@Fe-N-C	0.400	3.100	0.254	1.164

Uncategorized References

1.   G. Kresse and J. Furthmuller, *Comp. Mater. Sci.*, 1996, **6**, 15-50.
2.   G. Kresse and J. Furthmuller, *Phys. Rev. B*, 1996, **54**, 11169-11186.
3.   J. P. Perdew, K. Burke and M. Ernzerhof, *Phys. Rev. Lett.*, 1996, **77**, 3865-3868.
4.   G. Kresse and D. Joubert, *Phys. Rev. B*, 1999, **59**, 1758-1775.
5.   H. J. Monkhorst and J. D. Pack, *Phys. Rev. B*, 1976, **13**, 5188-5192.
6.   J. Park, M. Risch, G. Nam, M. Park, T. J. Shin, S. Park, M. G. Kim, Y. Shao-Horn and J. Cho, *Energy & Environmental Science*, 2017, **10**, 129-136.
7.   L. Zhuang, Y. Jia, H. Liu, X. Wang, R. K. Hocking, H. Liu, J. Chen, L. Ge, L. Zhang, M. Li, C.-L. Dong, Y.-C. Huang, S. Shen, D. Yang, Z. Zhu and X. Yao, *Advanced Materials*, 2019, **31**, 1805581.
8.   Y. Pei, W. He, M. Wang, J. Wang, T. Sun, L. Hu, J. Zhu, Y. Tan and J. Wang, *Chemical Communications*, 2021, **57**, 1498-1501.
9.   Y. Dai, J. Yu, Z. Zhang, S. Zhai, C. Cheng, S. Zhao, P. Tan, Z. Shao and M. Ni, *ACS Applied Materials & Interfaces*, 2021, **13**, 61098-61106.
10.   Z. Hou, Z. Sun, C. Cui, D. Zhu, Y. Yang and T. Zhang, *Advanced Functional Materials*, 2022, **32**, 2110572.
11.   W. Feng, Y. Feng, J. Chen, H. Wang, Y. Hu, T. Luo, C. Yuan, L. Cao, L. Feng and J. Huang, *Chemical Engineering Journal*, 2022, **437**, 135456.
12.   Y. Gao, D. Zheng, Q. Li, W. Xiao, T. Ma, Y. Fu, Z. Wu and L. Wang, *Advanced Functional Materials*, 2022, **32**, 2203206.
13.   Q. Lu, X. Zou, X. Wang, L. An, Z. Shao and Y. Bu, *Applied Catalysis B: Environmental*, 2023, **325**, 122323.
14.   Z. Ma, S. Liu, N. Tang, T. Song, K. Motokura, Z. Shen and Y. Yang, *ACS Catalysis*, 2022, **12**, 5595-5604.
15.   Z. Li, W.-J. Kang, H. Liu, X.-W. Du, F. Wang, Y. Song, Y. Liu, D.-L. Sun and F. Fang, *Advanced Functional Materials*, 2023, **33**, 2301947.
16.   G. Kumar, S. K. Das, C. Nayak and R. S. Dey, *Small*, 2024, **20**, 2307110.
17.   F. Zhang, R. Ji, X. Zhu, H. Li, Y. Wang, J. Wang, F. Wang and H. Lan, *Small*, 2023, **19**, 2301640.
18.   T. Zhou, W. Wang, H. Luo, Y. Wu, R. Xia, Y. Zhang, Z. Li, G. Jia, T. Zhang, H. Peng and Z. Guo, *ACS Catalysis*, 2024, **14**, 9313-9322.
19.   X. Zou, Q. Lu, J. Wu, K. Zhang, M. Tang, B. Wu, S. She, X. Zhang, Z. Shao and L. An, *Advanced Functional Materials*, **n/a**, 2401134.
20.   Y. Pan, Y. Li, A. Nairan, U. Khan, Y. Hu, B. Wu, L. Sun, L. Zeng and J. Gao, *Advanced Science*, 2024, **11**, 2308205.